Inorganic Chemistry

Article

pubs.acs.org/IC

Uncovering the Role of Intra- and Intermolecular Motion in Frustrated Lewis Acid/Base Chemistry: *Ab Initio* Molecular Dynamics Study of CO_2 Binding by Phosphorus/Boron Frustrated Lewis Pair [$tBu_3P/B(C_6F_5)_3$]

Maoping Pu and Timofei Privalov*

Department of Organic Chemistry, Stockholm University, Arrhenius Laboratory, Stockholm 10691, Sweden

Supporting Information

ABSTRACT: The role of the intra- and intermolecular motion, i.e., molecular vibrations and the relative motion of reactants, remains largely unexplored in the frustrated Lewis acid/base chemistry. Here, we address the issue with the *ab initio* molecular dynamics (AIMD) study of CO_2 binding by a Lewis acid (LA) and a Lewis base (LB), i.e., $tBu_3P + CO_2 + B(C_6F_5)_3 \rightarrow tBu_3P{-}C(O)O{-}B(C_6F_5)_3$ ([**1**]). Reasonably large ensemble of AIMD trajectories propagated at 300 K from structures in the saddle region as well as trajectories propagated directly from the reactants region revealed an effect arising from significant recrossing of the saddle area. The effect is that transient complexes composed of weakly interacting reactants nearly cease to progress along the segment of the minimum energy pathway (MEP) at the saddle region for a (subpicosecond) period of time during which the dominant factor is the light-to-heavy type of relative motion of the vibrating reactants, i.e., the "bouncing"-like movement of CO_2 with respect to much heavier phosphine and borane as main contributor to the mode that is perpendicular to the MEP-direction. In terms of how P···C and B···O distances change with time, the roaming-like patterns of typical AIMD trajectories, reactive and nonreactive alike, extend far beyond the saddle region. In addition to the dynamical portrayal of [**1**], we provide the energy-landscape perspective that takes into account the hierarchy of time scales. The verifiable implication of the effect found here is that the isotopically substituted (heavier) LB/LA "pair" should be less reactive that the "normal" and thus lighter counterpart.

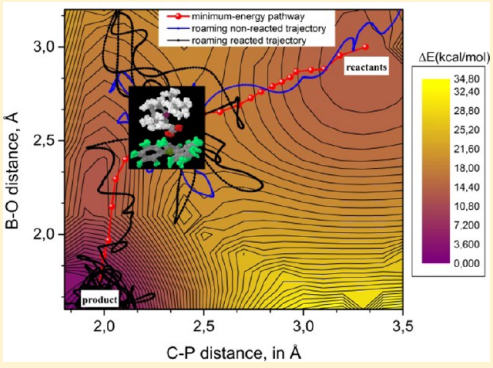

1. INTRODUCTION

Carbon dioxide (CO_2) is one of several chemical species which are responsible for the greenhouse effect in the earth's atmosphere. At present, the annual volume of the anthropogenic CO_2 emissions is still alarmingly high. Concerns about the future of the earth's climate motivate the interdisciplinary research of chemical techniques aiming at benign capture and storage, as well as transformation of CO_2 into usable chemicals.[1−3] From this viewpoint, an interesting and possibly technologically relevant reaction is CO_2 binding by the frustrated Lewis pair (FLP) $tBu_3P/B(C_6F_5)_3$ at room temperature ([**1**]); the zwitterionic adduct $tBu_3P{-}C(O)O{-}B(C_6F_5)_3$ dissociates at moderately elevated temperature (80 °C).[4,5]

$$tBu_3P + B(C_6F_5)_3 \xrightarrow{CO_2} tBu_3P{-}C(O)O{-}B(C_6F_5)_3\ [\mathbf{1}]$$

Lewis bases (LBs) and Lewis acids (LAs) such as tBu_3P and $B(C_6F_5)_3$ are too bulky to form a quenched Lewis adduct, hence, the concept of frustrated Lewis pairs (FLPs). Despite being relatively new, it applies to a wide range of LB/LA combinations.[6,7] Besides [**1**], FLPs bind N_2O and SO_2,[8−11] form adducts with relatively small olefins,[12] and heterolytically cleave H_2;[6,13−15] the latter is a part of interesting transfer−hydrogenation chemistries.[16]

A seminal paper by Stephan et al.[6] has sparked vivid interest in mechanisms of reactions involving FLPs and has led to further discoveries.[16] Progress has been made with regard to the rationalization of FLP-chemistries both with experiment and theory although the reactivity model is still actively debated.[17−20] Current conceptual base is limited in part because analyses of FLP reactions from the viewpoint of dynamics have not been performed until very recently: awareness of possible dynamical effects has just recently begun to rise.[19−23] Still, the most commonly used quantum chemical approach to mechanisms of FLP reactions is inherently time-independent, i.e., the minimum energy pathway (MEP) mapping of the potential energy surfaces (PESs) and thermodynamics considerations.[17,18]

Here, we investigate the role of the intra- and intermolecular motion, i.e., molecular vibrations and the relative motion of reactants, in the mechanism of [**1**] with the direct *ab initio* molecular dynamics (AIMD) simulations at finite (nonzero)

Received: February 4, 2014
Published: April 15, 2014

   dx.doi.org/10.1021/ic500284q | *Inorg. Chem.* 2014, 53, 4598−4609

temperature and PES exploration. For an accurate description of both covalent and noncovalent interactions, we use the current level of the dispersion-corrected density functional theory (DFT-D);[24] computational details are described in section 2. In a broad sense of the question about mechanistic role of multiscale nuclear motion in chemical and enzymatic reactions, the work presented herein relates to prior investigations of the post-transition state dynamics in large chemical systems,[25] the role of protein dynamics in enzyme catalysis,[26−29] nucleophilic substitution (S_N2) reactions,[30,31] and mechanisms of roaming reactions.[32−34] Theory of the heavy−light−heavy (HLH) reactions is also relevant for the work presented herein.[35]

Specifically, our idea is that a combination of factors (i.e., the difference of intrinsic time scales of the intra- and intermolecular motion in $\{t\mathrm{Bu_3P} + \mathrm{CO_2} + \mathrm{B(C_6F_5)_3}\}$ system, the character of modes describing the relative motion of reactants in transient $t\mathrm{Bu_3P}\cdots\mathrm{C(O)O}\cdots\mathrm{B(C_6F_5)_3}$ complexes, the character and direction of the intrinsic reaction coordinate (IRC) in the configurational space and the shape of the saddle region) could lead to mechanistically significant transition state recrossing dynamics with verifiable implications. Specific origins of such an idea are as follows. In light of the results from a recent AIMD study of the mechanism of H_2 cleavage by $t\mathrm{Bu_3P}/\mathrm{B(C_6F_5)_3}$ pair,[19] one can expect that an interplay between the vibrational modes of CO_2, $t\mathrm{Bu_3P}$, and $\mathrm{B(C_6F_5)_3}$ may play a role in the mechanism of [**1**]. Due to the mass differences between coreactants, i.e., relatively light CO_2 versus considerably heavier $t\mathrm{Bu_3P}$ and $\mathrm{B(C_6F_5)_3}$, one can expect that the hierarchy of time scales of the relative motion of reactants could be mechanistically significant. On the basis of the time-independent energy landscape perspective of [**1**],[36] we expect some sort of coupling between IRC and modes which are perpendicular to the MEP-direction in the broad saddle region of PES; at the very least, one can anticipate some degree of "wandering" between nearly degenerate transition states which form a distribution in the broad and relatively flat saddle region.

The paper is organized as follows. All essential methodological aspects are described in Computational Methodology; additional details are provided in Supporting Information (SI). Background concisely presents most essential information about the minimum energy pathway of [**1**]. Results and Discussion presents all our results, both AIMD- and PES-based, and a concise discussion of thereof. In section 5, we specifically discuss general implications of the theory presented herein. The Concluding Remarks complete the paper.

2. COMPUTATIONAL METHODOLOGY

AIMD Methodology. Molecular dynamics simulation is becoming an important tool for understanding the physical (microscopic) basis of molecular interactions in many areas of chemistry.[27,37−40] Here, the a*b initio* molecular dynamics (AIMD) simulations were carried out with full account of the multidimensional potential energy surface (PES) provided by the Born−Oppenheimer energy. The latter is updated "on the fly" with each time step of the integration of Newton's equations of nuclear motion (with the velocity Verlet integration algorithm). The AIMD implementation employed here, i.e., the commercially available package TeraChem,[41] allows for accurate trajectory-propagation either with the conservation of the total energy (potential energy plus kinetic energy) or with the constant-temperature algorithm in the form of the Langevin thermostat, that is, NVE (microcanonical ensemble) or NVT (canonical ensemble) dynamical schemes. The NVT scheme using the Langevin thermostat with the damping time τ is useful for describing a slow energy transfer between the (reacting) solute and the solvent bath. Our approach to nuclear motion is nonquantized, i.e., fully classical motion of atoms. The fully quantized molecular dynamics is impractical at present due to the size of the $\{t\mathrm{Bu_3P} + \mathrm{CO_2} + \mathrm{B(C_6F_5)_3}\}$ system. The quasiclassical approach that assigns the zero-point vibrational energy to the harmonic modes of vibrations as initial conditions was not adopted for reasons described in Supporting Information.

Ensemble of AIMD Trajectories. The main body of results presented in this Article is based on an ensemble of 125 NVE trajectories of fixed duration (2.5 ps per trajectory) propagated with the time-step of 1 fs from the transition state of CO_2 binding by $t\mathrm{Bu_3P}$ and $\mathrm{B(C_6F_5)_3}$ molecules (TS-structure in Supporting Information Figure S1) using standard sampling of the initial velocities within the Maxwell−Boltzmann distribution at 300 K. After assignment of initial velocities, the center of mass motion was removed. Out of 125 trajectories initiated at TS-structure, 28 trajectories have reached the product-area while the rest of the trajectories retreated to the reactants-area; all trajectories stayed in respective areas which they have reached. Our statistical analysis is based on the ensemble of 312 500 AIMD snapshots of all 125 NVE trajectories propagated from the TS-structure. We have checked that the total energy (potential energy plus kinetic energy) was well-conserved for NVE trajectories irrespective of areas they have eventually reached (product- or reactants-areas). For diagnostics, a representative subset of NVE trajectories has been compared with NVT dynamics using Langevin thermostat with the typical solvent−solute relaxation time $\tau \approx 2$ ps. No changes worth mentioning have been observed. Also, we have checked that the pattern of dynamics is insensitive to the choice of the initial structure within the saddle area of PES.

NVE Trajectory-Propagation from the Reactants-Area. Mainly for diagnostics, we have performed reversal of a few randomly selected NVE trajectories which retreated to the reactants-area from the initial TS-structure; thermodynamic detailed balance and time-reversibility of classical equations of atomic motion allows for that. In the reactants-area where $t\mathrm{Bu_3P}$, $\mathrm{B(C_6F_5)_3}$, and CO_2 are nearly separated, snapshots of both the geometry and all atomic velocities of randomly selected trajectories which originated from the TS-structure were taken followed by the reversal of all velocities. Thus, obtained coordinates and velocities of atoms in $\{t\mathrm{Bu_3P} + \mathrm{CO_2} + \mathrm{B(C_6F_5)_3}\}$ system served as initial conditions for new NVE trajectories heading from the reactants-area toward and eventually into the saddle area.

Level of Theory. Calculations have been carried out with the system formally in gas phase and with BLYP density functional in AIMD simulations for reasons of balancing computational costs and accuracy, the same as in the density functional PES calculations. The dispersion-correction developed by Grimme et al.[24] with fairly large split-valence triple-ζ basis set 6-311g** with the polarization functions on all atoms has been used.

RMSD. In the analysis of trajectories, we use the root mean squared deviation (RMSD):

$$\mathrm{RMSD}(t, t_0) = \sqrt{\frac{\sum_i^N [\vec{r}_i(t) - \vec{r}_i(t_0)]^2}{N}} \qquad (1)$$

In eq 1, $\vec{r}_i(t)$ is the position-vector of atom i at time t along trajectory, and the sum includes either all N atoms or a select group of particular interest; the reference structure corresponds to time t_0. The initial TS-structure (Supporting Information Figure S1) is our reference, i.e., $t_0 = 0$ in eq 1; we exclude all hydrogen atoms from the sum in eq 1in order to simplify RMSD analysis of full AIMD ensemble of 312 500 structures.

3. BACKGROUND: THE MINIMUM ENERGY PATHWAYS OF CO_2 BINDING

Prior to presenting the dynamical analysis of [**1**], let us briefly review the minimum energy pathways (MEPs) of CO_2 binding by $t\mathrm{Bu_3P}/\mathrm{B(C_6F_5)_3}$ pair calculated with the climbing image

dx.doi.org/10.1021/ic500284q | Inorg. Chem. 2014, 53, 4598−4609

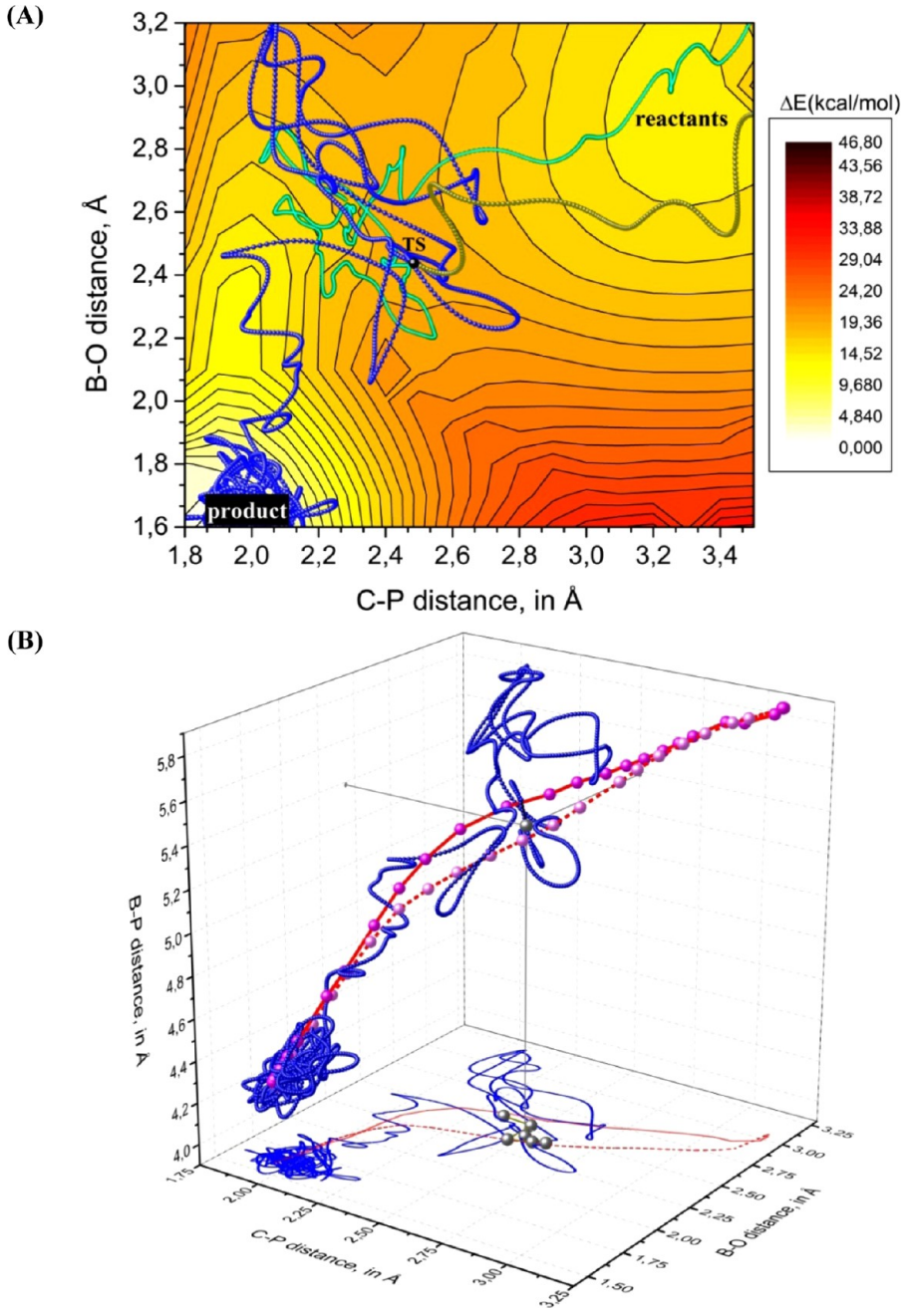

Figure 1. (A) Representative AIMD trajectories of the evolution of $\{t\mathrm{Bu_3P} + \mathrm{CO_2} + \mathrm{B(C_6F_5)_3}\}$ system from the TS-structure to the product and to the reactants region (blue and green, respectively). The reverse-propagated counterpart of the reactive trajectory is in dark yellow. The contour line spacing of E(P···C, B···O) is 1.2 kcal/mol, i.e., $\approx 2\ k_BT$ at 300 K, and k_B is the Boltzmann constant. (B) A comparison of the reactive trajectory (blue) with boundaries of the ensemble of MEPs (solid and dashed red lines); the TS-structure from Supporting Information Figure S1 and C−P/B−O projections of other TSs are in gray.[36]

nudged elastic band method (CI-NEB) in our recent study.[36,42−44]

$$\{t\mathrm{Bu_3P} + \mathrm{CO_2} + \mathrm{B(C_6F_5)_3}\}^{\mathrm{vdW}} \rightarrow t\mathrm{Bu_3P{-}C(O)O{-}B(C_6F_5)_3}\ [\mathbf{2}]$$

Following the routine procedure for MEP-mapping of PES, reaction of [**1**] can be represented by a simplified description (**2**) where the geometry-optimized van der Waals (vdW) complex composed of all coreactants, i.e., $\{t\mathrm{Bu_3P} + \mathrm{CO_2} + \mathrm{B(C_6F_5)_3}\}^{\mathrm{vdW}}$, is the starting point. In our earlier PES mapping,[36] starting points of MEPs were optimized snapshots from AIMD simulations of $\{t\mathrm{Bu_3P} + \mathrm{CO_2} + \mathrm{B(C_6F_5)_3}\}^{\mathrm{vdW}}$. An example of typical transition-state (TS) structure and the two-dimensional PES of $\{t\mathrm{Bu_3P} + \mathrm{CO_2} + \mathrm{B(C_6F_5)_3}\}$ system, E(P···C, B···O), are shown in the Supporting Information (Figure S1). On Figure 1, E(P···C, B···O) is shown on the background of the trajectory-plots with the contour line spacing of 1.2 kcal/mol; the chosen contour line spacing is about 2 k_BT at 300 K where k_B is the Boltzmann constant. Additional information about the MEP-picture of CO_2 binding is presented in Supporting Information (Figures S2−8).

The overall reaction pathway of **2** is given by an ensemble of MEPs with meaningfully distinct TSs forming a distribution in

dx.doi.org/10.1021/ic500284q | Inorg. Chem. 2014, 53, 4598−4609

Scheme 1. Qualitative Decomposition of the Intrinsic Reaction Coordinate (IRC) of CO_2 Binding

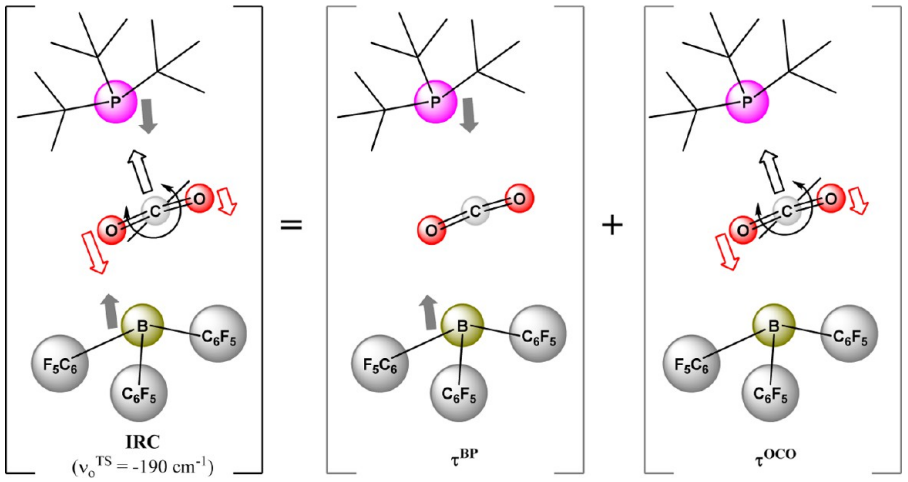

the shallow saddle area of multidimensional PES. The lack of curvature of PES along the intrinsic reaction coordinate (IRC) in the wide saddle area of PES, e.g., E(P···C, B···O) in Supporting Information Figure S1, is an indication that interactions between coreactants are rather weak and that the TS-configuration $\{t\mathrm{Bu_3P}\cdots\mathrm{C(O)O}\cdots\mathrm{B(C_6F_5)_3}\}^{TS}$ is not really "unique", and is, hence, an ensemble of TSs. Major components of IRC are $t\mathrm{Bu_3P} \leftrightarrow \mathrm{B(C_6F_5)_3}$ "breathing" mode and the CO_2 bending vibrational mode (Scheme 1); the corresponding time scales τ^{BP} and τ^{OCO} will be discussed further on in connection with the dynamical picture of CO_2 binding (*vide infra* sections 4.1 and 4.3). The harmonic frequency spectrum of representative TS-structure (Supporting Information Figure S1) has $\nu_o^{TS} \approx -190\ cm^{-1}$. Considering masses associated with major IRC-components (Scheme 1), it is understandable that ν_o^{TS} has a relatively small magnitude. In general, MEPs of **2** involve shortening of B···P distance from 5.91 Å (the initial vdW-complex) to 4.25 Å (the product); formation of P−C and B−O bonds is overall described as an asynchronous process. In the TS-region, the Wiberg bond indexes (WBIs) of P−C and B−O bonds are ≈80% and ≈30% of those in the product (Supporting Information Figure S3).

4. RESULTS AND DISCUSSION

4.1. Dynamics of Interactions of CO_2 with $t\mathrm{Bu_3P}$ and $\mathrm{B(C_6F_5)_3}$. To probe dynamics of the chemical step in [**1**], we have computed an ensemble of 125 AIMD trajectories at 300 K as described in section 2. Typical trajectories of the evolution of $\{t\mathrm{Bu_3P} + CO_2 + \mathrm{B(C_6F_5)_3}\}$ system from the TS-structure to the product and to the reactants region are shown in Figure 1A in blue and green, respectively; the reverse-propagated counterpart of the trajectory in blue is shown in dark yellow in Figure 1A. The two-dimensional PES E(P···C, B···O) is at the background of the trajectory-plots in Figure 1A.

On Figure 1B, typical reactive trajectory (the trajectory in blue from Figure 1A) is plotted against the outline of the ensemble of MEPs and the distribution of TSs in the saddle region.[36] Figure 2 shows only essential details of typical reactive trajectory; the dihedral angles of boron, the total dipole moment *d*, selected Mulliken atomic charges, and the RMSD-histogram are presented in Supporting Information (Figures S9−11).

Both reactive and nonreactive trajectories propagated from the saddle area have been typically observed to stray far away from MEP for subpicosecond duration, about 0.75 ps for trajectories in blue and green in Figure 1A. The saddle area recrossing has relatively large magnitude in accordance with the spatial dimensions of the phosphine···borane donor−acceptor "pocket", i.e., $|\Delta(\mathrm{P}\cdots\mathrm{C})| \approx |\Delta(\mathrm{B}\cdots\mathrm{O})| \approx 1.25$ Å, and involves extended excursions to regions afar from the saddle area (Figures 1 and 2). In terms of the evolution of C···P and B···O distances with time, it is intuitively reasonable to generally describe such patterns as "roaming phases".

Data clearly indicates that dynamics of a light molecule occurs on the "background" of a relatively slower dynamics of the heavier coreactants (Figure 2a−d). Note that after the initial rise to 0.6−0.7 Å level during the first few hundred femtoseconds, the RMSD curve of representative reactive trajectory has a relatively long flat segment with fluctuations which are similar to those in the product area, i.e., $\delta_x \approx \delta_{prod}$ in Figure 2d. On Figure 3, AIMD snapshots illustrate "turning-points" at which the direction of the trajectory-propagation reverses (see the trajectory in blue in Figure 1) due to collisions of CO_2 with either $t\mathrm{Bu_3P}$ or $\mathrm{B(C_6F_5)_3}$. As illustrated in Figure 3, the delocalization of the lone pair of phosphorus arises in AIMD snapshots with a relatively short P···C distance, i.e., P···C ≈ 2 Å; the magnitude of the total dipole moment could be used as an indication of the resultant donor−acceptor interactions.

The AIMD data presented above illustrates that (i) time scales of the IRC components, i.e., $t\mathrm{Bu_3P} \leftrightarrow \mathrm{B(C_6F_5)_3}$ "breathing" mode and bending of CO_2 (Scheme 1), are such that $\tau^{BP} > \tau^{OCO}$, and (ii) there is indeed certain latency of the progression along IRC; the $\{t\mathrm{Bu_3P} + CO_2 + \mathrm{B(C_6F_5)_3}\}$ system does not descend from the TS-structure to the product (or to the reactants-area) in a straightforward fashion. Amplitudes of relatively fast translational and ro-vibrational motions of CO_2 in weakly interacting $t\mathrm{Bu_3P}\cdots\mathrm{C(O)O}\cdots\mathrm{B(C_6F_5)_3}$ configurations which head toward the product or the reactants-area are limited by the overall shape and spatial dimensions of the slowly adjusting phosphine−borane donor−acceptor pocket.

The trajectory-patterns to which were refer here as "roaming phases" (Figures 1 and 2) arise because a particular mode of multiscale motion, i.e., the "roaming mode", is dynamically counteracting the potential energy driving force along the IRC-direction. Primarily, straying away from the IRC-direction occurs due to the "bouncing"-like motion of CO_2 between phosphine and borane (Figure 3c). Sideways CO_2 movements

dx.doi.org/10.1021/ic500284q | Inorg. Chem. 2014, 53, 4598−4609

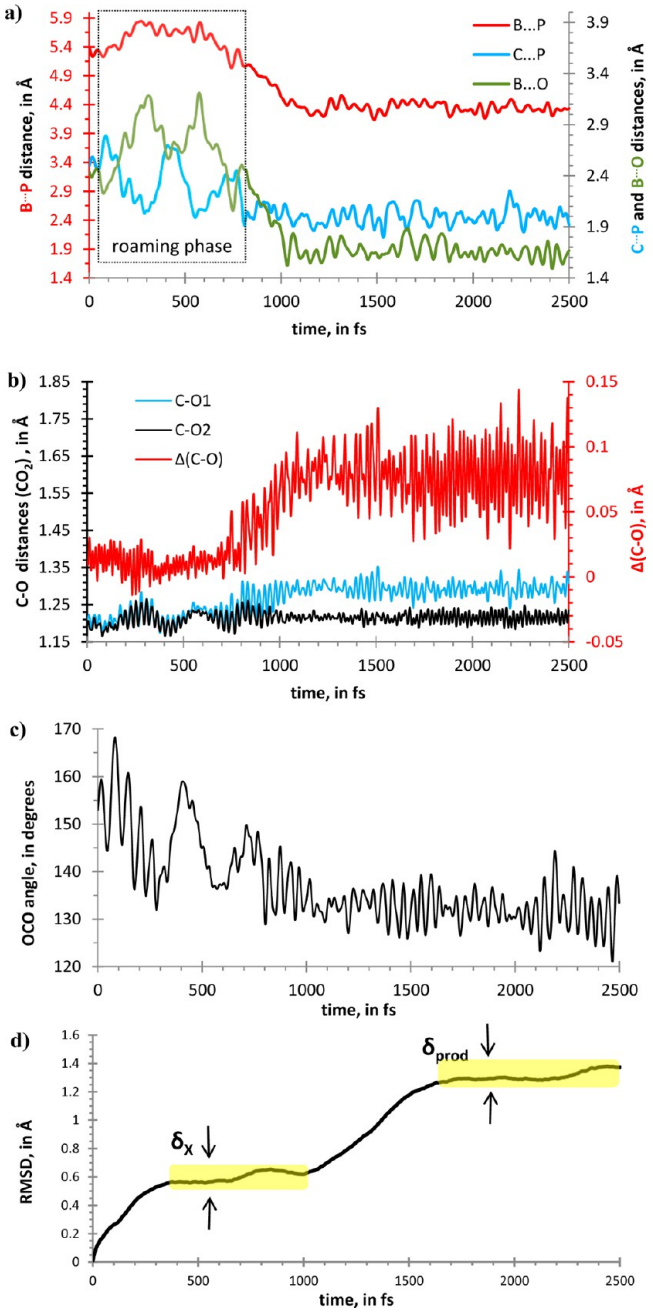

Figure 2. Selected geometrical parameters of the trajectory in blue from Figure 1: (a) B···P, C···P, and B···O distances; (b) C−O bonds in CO_2; (c) OCO angle; (d) RMSD curve (eq 1) with respect to the TS-structure from Supporting Information Figure S1. All distances and RMSD are in Å, time is in fs, and OCO angle is in degrees.

causes some back-and-forth "jiggling" along IRC. Movement of CO_2 is accompanied by the vibrational variation of the pyramidality of $B(C_6F_5)_3$ and vibrations of phosphorus in tBu$_3$P.[45] Less important contributors to the "roaming mode" are the low-amplitude P···C(O)O···B torsions coupled to limited rotations around the P···C "axis" and relatively fast intrinsic vibrations of C═O bonds in CO_2. The coupling between IRC (Scheme 1) and the "roaming mode" is dynamical in nature because sequential tBu$_3$P ↔ CO_2 and C(O)O ↔ $B(C_6F_5)_3$ collisions make non-negligibly slowing impact on the closing of the phosphine···borane "pocket". Among all trajectories, it was not uncommon to observe that movements

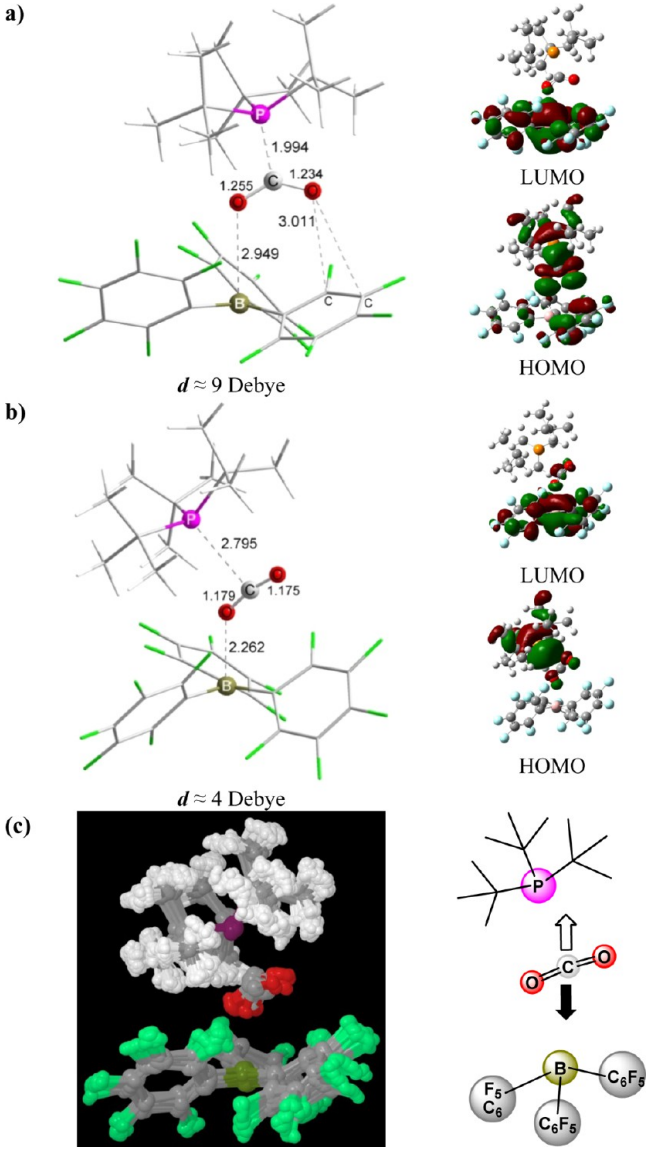

Figure 3. (a, b) Representative AIMD snapshots illustrating "turning points" of roaming phase (the trajectory in blue in Figure 1). (c) An overlay of 750 AIMD snapshots from the roaming phase with the simplified portrayal of the "bouncing"-like motion of CO_2 relative to tBu$_3$P and $B(C_6F_5)_3$.

of CO_2 within the evolving {tBu$_3$P + CO_2 + $B(C_6F_5)_3$} complex could cause tBu$_3$P and $B(C_6F_5)_3$ to completely part ways during roaming phases thus causing trajectory to retreat to the reactants region (*vide infra*).

A key point here is that IRC/MEP suggests that the passage through the saddle region involves *monotonous closing* of the phosphine···borane "pocket" with not fully synchronous but *matched shortening of both* tBu$_3$P···CO_2 and C(O)O···$B(C_6F_5)_3$ distances in accordance with the PES profile, i.e., E(P···C, B···O). That is *not* how the process goes with the account of the kinetic energy of all three reactants, i.e., at 300 K in actual AIMD simulations. In a nutshell, the dynamical effect found here is that at room temperature CO_2 moves within a rather loose phosphine···borane pocket and sequential tBu$_3$P ↔ CO_2 and C(O)O ↔ $B(C_6F_5)_3$ collisions either markedly suspend or completely disrupt closing of the phosphine···borane "pocket" despite the driving force along IRC. The donor−acceptor

dx.doi.org/10.1021/ic500284q | Inorg. Chem. 2014, 53, 4598−4609

interactions in the reacting complexes do take place as indicated by the appearance of a relatively large dipole moment of about 4−9 D. However, collisions suspend the closure of the phosphine···borane "pocket" and thus give rise to the characteristically flat segment of RMSD curves as illustrated in Figure 3: because of that, we think that "idling transient configurations" is a suitable term to describe the phenomenon. Note, however, that "idling" refers only to the temporarily suspended closure of the phosphine···borane "pocket" but not to the active movements of CO_2 with respect to the phosphine and borane. In terms of how C···P and B···O distances behave as functions of time, the manifestation of "idling transient configurations" is the roaming-like trajectory-pattern shaped orthogonally to the direction of IRC in the saddle region. Naturally, sequential tBu$_3$P ↔ CO_2 and C(O)O ↔ B(C_6F_5)$_3$ collisions correspond to the *mismatched* shortening of tBu$_3$P···CO_2 and C(O)O···B(C_6F_5)$_3$ distances, i.e., shortening of P···C distance together with the elongation of the O···B distance and *vice versa*. That type of motion is perpendicular to the direction of IRC in the saddle region of [**1**] (*vide infra*).

For diagnostic purposes and to add clarity to the discussion from above, we have calculated a number of trajectories starting directly from the reactants-area as described in section 2. Propagation of trajectories from the reactants-area affirmed main characteristics of trajectories propagated from the TS-structure. Typical nonreactive scenario is the passage of trajectory through the saddle of PES followed by one or several collisions of CO_2 with heavier coreactants which steer the evolution back into the reactants region; as noted earlier, it is not uncommon for movements of CO_2 to make tBu$_3$P and B(C_6F_5)$_3$ part ways. An example of that is the nonreactive trajectory in Figure 4 showing a passage through the saddle area of PES followed by (tBu)$_3$P + CO_2 collision and, about 150 fs later, CO_2 + B(C_6F_5)$_3$ collision; B···P distance remains at about 5.35 Å in the short duration of sequential collisional

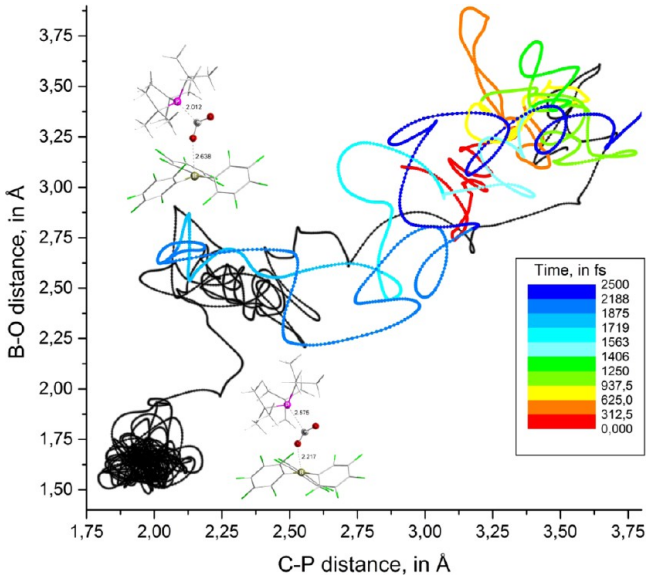

Figure 4. Representative reactive and nonreactive AIMD trajectories propagated from the reactants-area at 300 K as described in section 2. The reactive trajectory is in black, and the nonreactive trajectory is colored in accordance with the elapsed time. Two AIMD snapshots illustrate the closest (tBu)$_3$P···CO_2 and C(O)O···B(C_6F_5)$_3$ collisional encounters along the nonreactive trajectory.

interactions. As a result of those sequential collisions, the complex returns to the reactants-area. An opposite scenario is illustrated by the reactive trajectory plotted in Figure 4 with more details shown in Figure 5. In this case, sequential (tBu)$_3$P

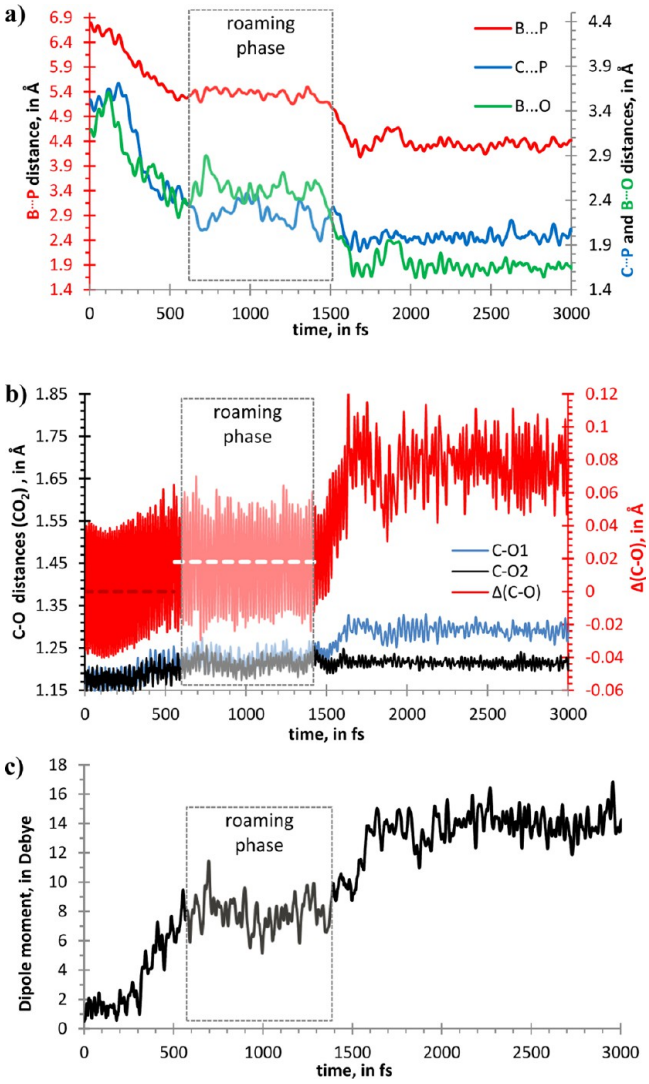

Figure 5. Details of representative trajectory of the evolution of {tBu$_3$P + CO_2 +B(C_6F_5)$_3$} system toward the product directly from the reactants-area of PES at 300 K (the trajectory in black in Figure 4): (a) B···P, C···P, and B···O distances; (b) C−O distances in CO_2; (c) the total dipole moment (in Debye). All distances are in Å; time is in fs.

+ CO_2 and CO_2 + B(C_6F_5)$_3$ collisions do take place, but the net result does not prevent the system from reaching the product region. Note that multiple large-amplitude passes through the saddle area due to (tBu)$_3$P + CO_2 and CO_2 + B(C_6F_5)$_3$ collisions form a typical pattern of a roaming phase, just as previously shown in Figure 1 for trajectories initiated from the saddle area. For the reactive trajectory plotted in Figure 4, the B···P distance remains at about 5.4 Å for the duration of the roaming phase (see also Figure 5); small-amplitude "wiggling" of trajectories in Figure 4 is caused by fast intrinsic vibrational motions in tBu$_3$P···C(O)O···B(C_6F_5)$_3$ complexes.

4.2. Statistical Analysis of Trajectories Initiated from the Saddle Region. For a global description of tBu$_3$P···C(O)O···B(C_6F_5)$_3$ configurations from reasonably large

dx.doi.org/10.1021/ic500284q | Inorg. Chem. 2014, 53, 4598−4609

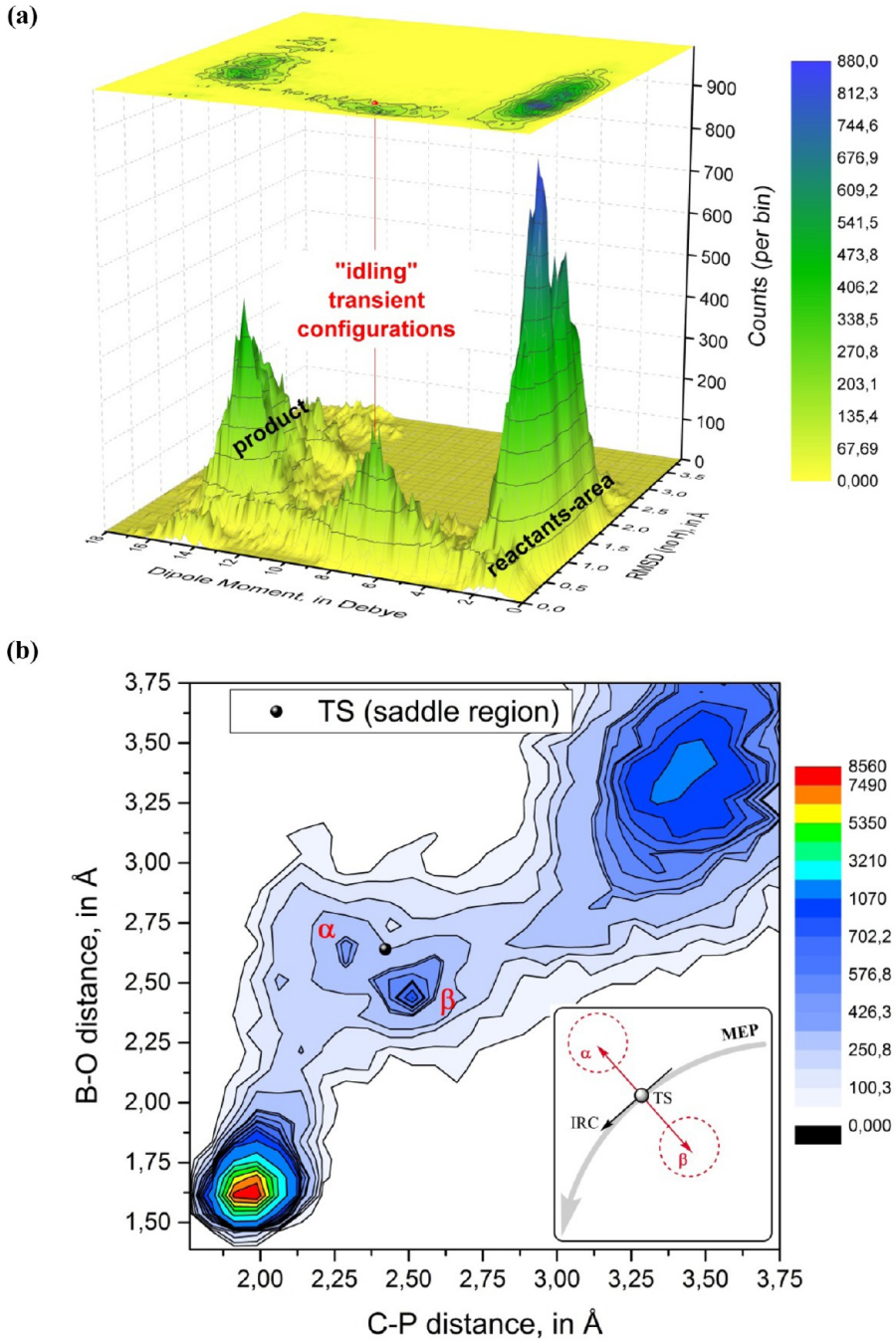

Figure 6. (a) Two-dimensional occurrence-histogram of the root mean squared deviations (RMSDs, in Å) and the total dipole moment (d, in Debye) of the AIMD snapshots from all trajectories initiated from the saddle area of PES; 312 500 AIMD snapshots are taken into account. The initial TS-structure (Supporting Information Figure S1) serves as a reference in RMSD calculations according to eq 1. (b) The occurrence of P···C/B···O distances in $\{t\mathrm{Bu_3P} + \mathrm{CO_2} + \mathrm{B(C_6F_5)_3}\}$ system based on AIMD trajectories initiated from the saddle point at 300 K. All distances are in Å.

ensemble of AIMD trajectories initiated from the saddle region, we have carried out the two-dimensional statistical analysis of RMSDs together with the total dipole moment, d. The two-dimensional RMSD/d histogram (Figure 6a) has three major features. The expected two features correspond to the dynamics of the product and vdW-complexes in the reactants-area: namely, $d \approx 14$ D together with RMSDs clustered around 1.4 Å and $d < 3$ D together with RMSDs broadly distributed around 1.5 Å. A statistically meaningful midway feature in Figure 6a is in the area 5 D < d < 9 D together with RMSDs distributed around 0.65 Å. All trajectory data unambiguously shows that "roaming" trajectory-phases are indeed responsible for the midway feature in Figure 6a. The relatively large magnitude of d indicates a separation of positive and negative charges and thus donor−acceptor interactions. The meaning of the midway feature in Figure 4 is the dynamically active but also temporarily idling state of the system that does not progress along the reaction coordinate (*vide supra*). For comparison of the selected structural characteristics of the ensemble of TSs, see our earlier work for details regarding the ensemble of TSs of [**1**],[36] with the whole set of AIMD snapshots contributing to the midway feature in Figure 6a given in Table S1 in Supporting Information.

dx.doi.org/10.1021/ic500284q | *Inorg. Chem.* 2014, 53, 4598−4609

In the statistical sense, motion of CO_2 within the phosphine···borane "pocket" indeed has oscillatory characteristics in the ensemble of all AIMD trajectories initiated from the saddle area, reactive and nonreactive alike. On the basis of 312 500 AIMD snapshots, the occurrence of P···C/B···O distances is shown as a contour plot of the two-dimensional histogram (Figure 6b).[46] Note that in the area corresponding to the "idling" transient $t\mathrm{Bu_3P}^{\cdots}\mathrm{C(O)O}^{\cdots}\mathrm{B(C_6F_5)_3}$ configurations which we have discussed above, the occurrence of P···C/B···O distances forms a distribution with two characteristic maxima (α and β in Figure 6b); α arises as statistical representation of $t\mathrm{Bu_3P} \leftrightarrow CO_2$ collisions, i.e., the turning points with the relatively short P···C but long B···O distances (Figure 3a), and β statistically represents $\mathrm{C(O)O} \leftrightarrow \mathrm{B(C_6F_5)_3}$ collisions (Figure 3b). Note also that the line that could be drawn through α and β in Figure 6b is orthogonal to the direction of IRC/MEP in the saddle region (see the illustrating insert in Figure 6b). Just as the classical harmonic oscillator is most likely to be found at either of its two turning points, the *alternating variations* of P···C and B···O distances during the subpicosecond roaming phases (crossing of the saddle region) give rise to the statistical picture shown in Figure 6b with maxima α and β.

Taking into account all from above, one can generalize our results for chemical systems of LB···X···LA type with markedly unequal masses of reactants; i.e., M(LB) and M(LA) are (much) larger than M(X) where X could be CO_2, N_2O, or SO_2, and flat saddle regions similar to the saddle region of $t\mathrm{Bu_3P}$···$\mathrm{C(O)O}$···$\mathrm{B(C_6F_5)_3}$ system. The expected manner in which reactive trajectories should cross the saddle region is illustrated in Scheme 2. Data presented in Figure 4 suggests that

Scheme 2. Simplified Portrayal of the Crossing of the Saddle Region by Typical Reactive Trajectory

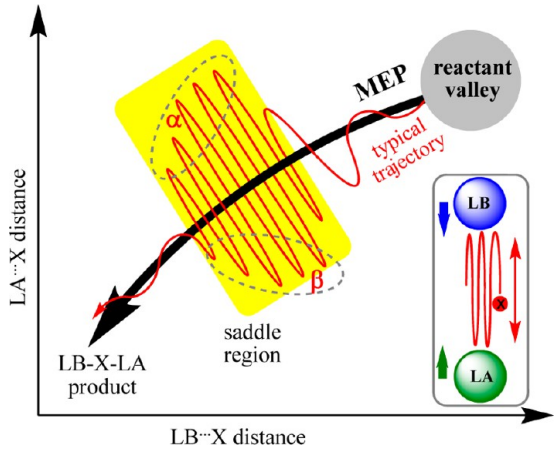

trajectories which return to the reactant valley, i.e., nonreactive trajectories, should as well contribute to the total ensemble of turning points.

4.3. Electronic-Structure Details about Interaction of CO_2 with $t\mathrm{Bu_3P}$ and $\mathrm{B(C_6F_5)_3}$. Let us now briefly examine the electronic structure picture of interactions between reactants (Figure 7). An interaction of the lone electron-pair of phosphorus, Lp(P), with the LUMO π^*-orbital of CO_2, $\pi^*(CO_2)$, gives rise to the $\{\mathrm{Lp(P)} + \pi^*(CO_2)\}$ molecular orbital, the highest occupied molecular orbital (HOMO) for all transient configurations. The lowest unoccupied orbital (LUMO) of transient $\{t\mathrm{Bu_3P} + CO_2 + \mathrm{B(C_6F_5)_3}\}$ configurations is localized on $\mathrm{B(C_6F_5)_3}$ with the boron-centered p-component "mixed" with the orbitals of the perfluoro aromatic rings. The electronic structure analysis of AIMD trajectories and representative MEP indicates that CO_2 binding is a charge-shift process,[47] involving phosphorus as the "primary donor". During roaming phases, electrostatic interactions between atoms with the partially positive and negative charge, i.e., $\mathrm{O}^{(\delta-)}/\mathrm{B}^{(\delta+)}$ and $\mathrm{O}^{(\delta-)}/\mathrm{C}^{(\delta+)}$ and $\mathrm{O}^{(\delta-)}/\mathrm{F}^{(\delta-)}$, are mechanistically important. At short-range B···P distances, boron together with the perfluoro aromatic rings accepts electron density from $\{\mathrm{Lp(P)} + \pi^*(CO_2)\}$ and possibly from the oxygen-centered occupied π orbitals of CO_2 (π(OCO)). Although at the DFT level of theory it is problematic to evaluate the relative weight of the two possible electronic configurations with either $\{\mathrm{Lp(P)} + \pi^*(CO_2)\} - \mathrm{LUMO(B(C_6F_5)_3)}$ or $\pi(\mathrm{OCO}) - \mathrm{LUMO(B(C_6F_5)_3)}$ molecular orbital interactions, both can be mechanistically important because $\{\mathrm{Lp(P)} + \pi^*(CO_2)\}$ and π(OCO) have a tendency to converge, since the perturbation theory energy-analysis of C(O)O···B interactions shows considerable magnitude of the second order interaction energy at the post-TS stage of CO_2 binding (Supporting Information Figures S7–8).

4.4. Adiabatic PES-Viewpoint on CO_2 Binding by $t\mathrm{Bu_3P}$ and $\mathrm{B(C_6F_5)_3}$. At first glance, $t\mathrm{Bu_3P}$ and $\mathrm{B(C_6F_5)_3}$ in TSs of [**1**], e.g., the TS-structure from Supporting Information Figure S1, are in a favorable conformation for capturing CO_2. That is not really the case according to molecular dynamics simulations; instead, there are significant roaming phases of trajectories together with the overall latency in progression of $\{t\mathrm{Bu_3P} + CO_2 + \mathrm{B(C_6F_5)_3}\}$ along IRC. Knowing modes of nuclear motion which make major contributions to IRC and "roaming", one can look at the energy-landscape picture of CO_2 binding by $t\mathrm{Bu_3P}$ and $\mathrm{B(C_6F_5)_3}$ from adiabatic point of view by considering the potential energy of $\{t\mathrm{Bu_3P} + CO_2 + \mathrm{B(C_6F_5)_3}\}$ as a function of P···C and B···O distances with the B···P distance as a parameter, 2D-PESs E(P···C, B···O|B···P) from Figure 8. Structures corresponding to local minima on 2D-PES plots of E(P···C, B···O|B···P) at selected values of B···P distance are shown in Figure S15 in Supporting Information.

For the B···P distances close to the value found in the TS-structure, $(\mathrm{B\cdots P})^{\mathrm{TS}} \approx 5.4$ Å, the shape of E(P···C, B···O|B···P) is such that only a very small energy-change arises from the contraction of P···C together with the elongation of B···O and *vice versa*, i.e., limited translational motion of CO_2 in-between $t\mathrm{Bu_3P}$ and $\mathrm{B(C_6F_5)_3}$ as major contributor to the "roaming" mode the *alternating variations* of P···C and B···O distances. In contrast to that, directions toward the area of the product-like P···C and B···O distances are met with steeply rising slope of E(P···C, B···O|B···P); the product-like energy-well begins forming on E(P···C, B···O|B···P) at B···P < 5.0 Å.

Data presented in Figure 8 supports the notion of the dynamically active, i.e., in terms of how P···C and B···O distances evolve, but also temporarily idling (suspended) state of the system that does not actually progress along the reactions coordinate. An overall direction of excursions outside of the saddle area in two-dimensional P···C/B···O space during roaming phases (Figure 1) is in accord with the potential energy landscapes shown in Figure 8; a specific region of the localized trajectory-orbiting generally corresponds to the shallow local minima located at relatively large P···C and B···O distances (also shown in Figure 8).

The B···P distance constraint corresponds to the limit $\tau^{\mathrm{BP}} \rightarrow \infty$ in the dynamical sense. Thus, τ^{BP} has the meaning of an effective "dynamical frustration" of the chemical step in [**1**]. As

dx.doi.org/10.1021/ic500284q | Inorg. Chem. 2014, 53, 4598–4609

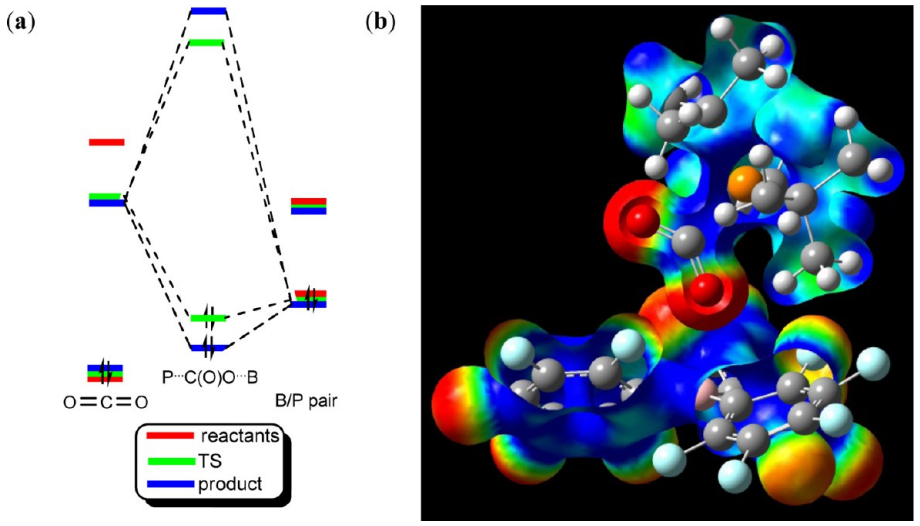

Figure 7. (a) Illustration of the frontier orbital interactions in the process of CO_2 binding by tBu_3P and $B(C_6F_5)_3$. Considered are the reactants composing the initial vdW complex, TS, and the product. Relative position of all MOs is in accordance with the orbital energies. For clarity, the occupied orbitals are indicated with the pair of up/down arrows. Background information is in Supporting Information. (b) The electrostatic potential (ESP) surface of representative transient configuration $tBu_3P\cdots CO(O)\cdots B(C_6F_5)_3$ from AIMD simulations; colors from red to dark blue represent ESP values from the lowest negative to the most positive, respectively.

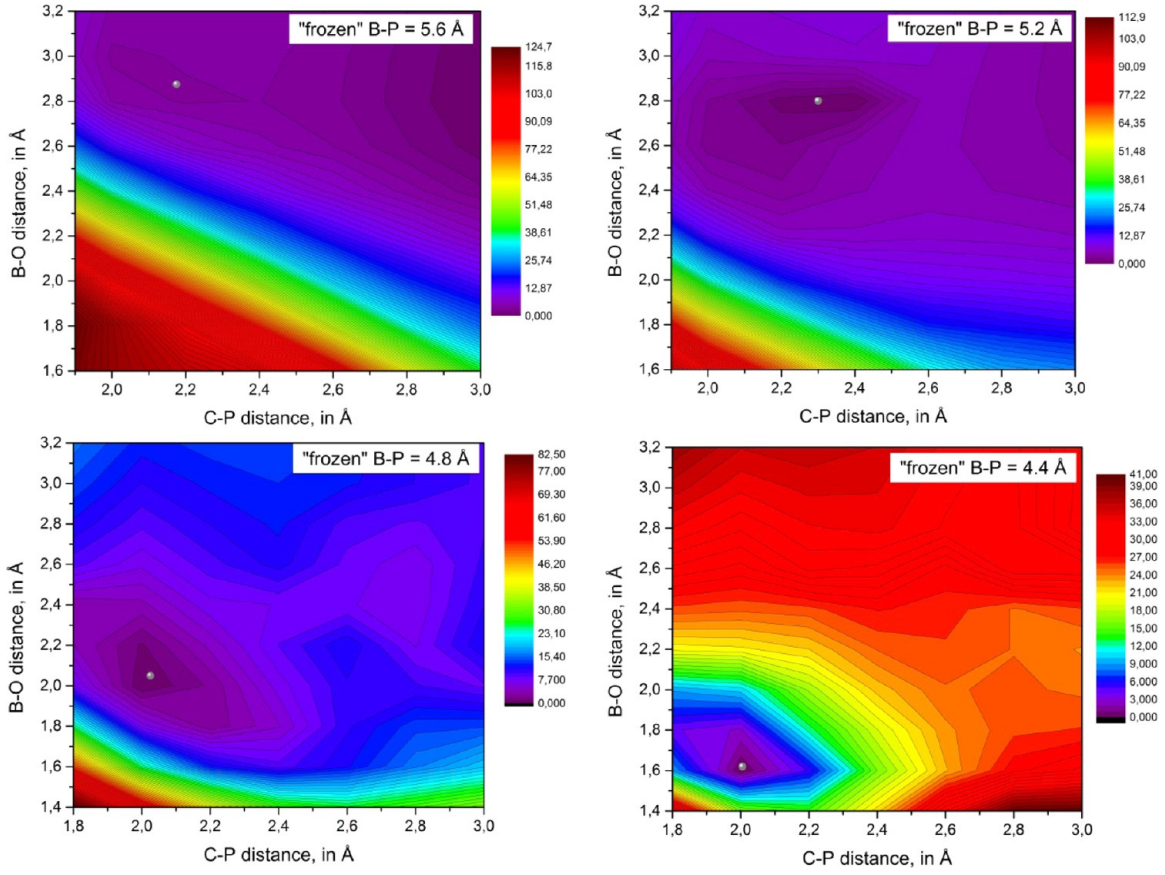

Figure 8. 2D-PESs E(P···C, B···O|B···P) at selected values of B···P distance; the potential energy is displayed relative to the marked local minimum (in kcal/mol). The contour line spacing is 1 kcal/mol.

explained earlier, τ^{BP} is mass-sensitive, and longer τ^{BP} should correspond to heavier LA and LB. Thus, isotopic substitution of $tBu_3P/B(C_6F_5)_3$ should in principle increase τ^{BP} and thus the latency of the progression along IRC toward the product. Therefore, one can expect lower reactivity of the isotopically heavier $tBu_3P/B(C_6F_5)_3$ pair versus the "normal" counterpart.

5. "AGILITY"–REACTIVITY RELATION FOR AN FLP

Since the discovery of the first FLP systems, the bulkiness of a Lewis acid (LA) and a Lewis base (LB) has been regarded as an essential safeguard of chemical reactivity which hinders the quenching into a Lewis adduct. However, bulkiness translates

dx.doi.org/10.1021/ic500284q | Inorg. Chem. 2014, 53, 4598–4609

into being heavy LA and LB, and thus perhaps a not so conformationally "nimble" LA/LB pair of molecule.

For CO_2 binding by tBu$_3$P and B(C$_6$F$_5$)$_3$ molecules, we show that the B···P distance as an exemplary geometrical characteristics of the phosphorus···boron "pocket" is dynamically coupled with the formation of P−C/B−O bonds. The latency of the tBu$_3$P ↔ B(C$_6$F$_5$)$_3$ mode of collective motion arises in part due to the combined inertia of tBu$_3$P and B(C$_6$F$_5$)$_3$ which relates to their molecular masses and also because of the dynamical IRC-coupling of what we call herein "roaming mode". Thus, the isotopically substituted (heavier) tBu$_3$P/B(C$_6$F$_5$)$_3$ pair is expected to be somewhat less reactive than the "normal" (lighter) counterpart. The ratio of rate constants in a chemical reaction using light versus heavy LA/LB pair should provide information about an effect arising from mass-induced differences in atomic (molecular) motions which we have described herein. In principle, calculated with the molecular dynamics the difference in the response time between the isotopically heavy and light FLP at different temperatures could be translated into the effective free-energy difference in the barrier heights for comparison with experimental results. However, at present there are no experimental data to motivate such an elaborate and costly theoretical study. Also, kinetic measurement using isotopic substitution of LA, LB, and CO_2 in combinations could provide even deeper insight into dynamical effects relevant for the chemical step in [**1**].

There is a recent example of a conceptually similar effect being validated with experimental methods albeit in a different area of chemistry, i.e., the case of dihydrofolate reductase catalysis.[26] The microscopic mechanisms responsible for the dynamical coupling effects described here and in the aforementioned study are similar. Key similarity is a scenario in which the difference in phenomenological rate constants between the heavy and light versions of a "chemical environment", i.e., enzyme with an active site and tBu$_3$P/B(C$_6$F$_5$)$_3$ pair with the phosphorus···boron "pocket" in our case, arises in part because of the different participation of motions responsible for the geometry of the "chemical environment" in the reaction coordinate. At it has been shown that isotopic substitution causes differences in environmental coupling to the chemical step and thus protein dynamics has a small but measurable effect on the chemical reaction rate of "normal" enzyme versus the heavy (^{15}N, ^{13}C, ^{2}H substituted) counterpart, the chemical step being slightly but measurably slower in the heavy enzyme.[26] That is quite similar to the prediction we make here (*vide supra*).

6. CONCLUDING REMARKS

We have performed *ab initio* molecular dynamics simulations of the process P(tBu)$_3$ + B(C$_6$F$_5$)$_3$ + CO_2 → tBu$_3$P−C(O)O−B(C$_6$F$_5$)$_3$ [**1**] at 300 K in gas phase using high level of quantum chemical description of both covalent and noncovalent interactions by the dispersion corrected density functional theory (DFT-D3). The main body of our work is based on an ensemble of AIMD trajectories which sufficiently elucidate both the binding scenario and the return to the reactants-area; trajectories were initiated from the saddle area of the potential energy surface (PES) of the {tBu$_3$P + CO_2 + B(C$_6$F$_5$)$_3$} system using standard sampling of the initial velocities within the Maxwell−Boltzmann distribution at 300 K.

From a general point of view, our results suggest a connection between an "agility" and chemical reactivity for a class of FLPs. Specifically, we show that the B···P distance in reacting {tBu$_3$P + CO_2 + B(C$_6$F$_5$)$_3$} is dynamically coupled with the evolution of P···C/B···O distances. A slightly larger latency of movement along the reaction coordinate is expected to arise from a larger mass-related latency of tBu$_3$P ↔ B(C$_6$F$_5$)$_3$ collective mode of motion in the isotopically heavier FLP. Kinetic measurements using isotopically "heavy" FLP versus the "normal" and thus lighter counterpart could be a way to verify the mechanism found here.

Speaking of details, the passage of {tBu$_3$P + CO_2 + B(C$_6$F$_5$)$_3$} through the saddle area of PES has been found to involve significant transition state recrossing dynamics with subpicosecond duration. The collective mode of motion involved in that has certain roaming characteristics and is coupled to IRC. A parallel process with roaming reaction pathways[32] is more tangible considering the reverse of [**1**]. Dissociation of tBu$_3$P−C(O)O−B(C$_6$F$_5$)$_3$ adduct at elevated temperature (≈100 °C) has been briefly examination in our recent study, and we have indeed found first indications of two main dissociation channels.[36] As illustrated by Figure S15 in the Supporting Information, CO_2 can undergo limited translational motion (roaming) between the separating tBu$_3$P and B(C$_6$F$_5$)$_3$. For completeness, let us also mention that characteristics of the "roundabout" mechanisms of S_N2 reactions[31] have similarities to the mechanism found here.

Herein presented molecular dynamics modeling of the chemical step in [**1**] did not include explicit solvent. In principle, solvent molecule(s) could compete with CO_2 for a space in the phosphorus···boron "binding pocket" at a stage of the merger of the first solvation shells of coreactants. Not to be ignorant of the matter but not yet technically capable to perform in-depth investigation, we have carried out exploratory AIMD simulations of CO_2 binding by tBu$_3$P and B(C$_6$F$_5$)$_3$ molecules in the extended molecular model including 30 explicit solvent molecules which sufficiently approximate the first collective solvation shell of the tBu$_3$P + CO_2 + B(C$_6$F$_5$)$_3$ system with tBu$_3$P···B(C$_6$F$_5$)$_3$ separation of up to 7 Å. Considering the exploratory nature of these simulations, details are presented in the Supporting Information (Figures S16−17). These solute−solvent cluster simulations indicate the following: (i) The hierarchy of van der Waals volumes of tBu$_3$P, CO_2, B(C$_6$F$_5$)$_3$ molecules and typical solvent molecule (toluene), i.e., V^{vdW}(LA), V^{vdW}(LB) ≫ V^{vdW}(solv) > V^{vdW}(CO_2), effectively hinders possible solvent−CO_2 competition. Qualitatively speaking, spatial dimensions of bulky tBu$_3$P and B(C$_6$F$_5$)$_3$ with separation of less than 6.5−7.0 Å provide an "umbrella of protection" for the phosphorus···boron binding pocket. (ii) Essential characteristics of roaming phases of "in-solvent" AIMD trajectories are in full accord with those based on modeling not using explicit solvent (*vide supra*) except that with tBu$_3$P and B(C$_6$F$_5$)$_3$ surrounded by explicit solvent the phosphorus···boron pocket has an appreciably larger conformational inertia, and thus duration of the observed roaming phases of "in-solvent" AIMD trajectories typically was slightly on the upper side of 2 ps.

Let us conclude by saying that it has been realized quite early on that, in addition to thermodynamics factors, i.e., the total energy change and the TS-barrier heights which are reasonably well-described by the nondynamical (static) potential energy approach, dynamics ought to be considered as well in order to fully understand and creatively use reactivity of FLPs. A similar sentiment has been first expressed in connection to the mechanisms of H_2 activation by FLPs a few year ago.[17c] However, for a considerable period of time matters of kinetics

dx.doi.org/10.1021/ic500284q | Inorg. Chem. 2014, 53, 4598−4609

and dynamics in FLP-chemistries have not received due attention neither from experimentalists nor theoreticians. Results presented herein uncover for the first time fundamentals of an intricate dynamical coupling effect on the chemical step in an FLP involving reaction; we do suspect that this reveals only a tip of an iceberg and believe that a fertile area lies ahead with regard to further investigations of effects of dynamics on FLP chemistries.

■ ASSOCIATED CONTENT

Supporting Information

Computational and technical details supplementary to the Methodology section, additional methodology-related references, relevant background information regarding the MEP of CO_2 binding (Figures S1−8), additional information for representative AIMD trajectories and the statistical analysis of trajectories (Figures S9−13), additional information for PESs from Figure 8 (Figure S14), illustration of AIMD trajectories of the dissociating tBu$_3$P−C(O)O−B(C$_6$F$_5$)$_3$ adduct (Figure S15), details about an exploratory in-solvent AIMD simulations of CO_2 interactions with and binding by tBu$_3$P and B(C$_6$F$_5$)$_3$ molecules (Figures S16−17), and supplementary tables (Tables S1−3). This material is available free of charge via the Internet at http://pubs.acs.org.

■ AUTHOR INFORMATION

Corresponding Author

*E-mail: priti@organ.su.se.

Notes

The authors declare no competing financial interest.

■ ACKNOWLEDGMENTS

Financial support from Berzelius Center EXSELENT and Knut and Alice Wallenberg foundation. A part of the calculations was performed on resources provided by the Swedish National Infrastructure for Computing (SNIC) at the National Supercomputer Center (NSC).

■ REFERENCES

(1) (a) Kaufman, D. G.; Franz, C. M. *Biosphere 2000: Protecting Our Global Environment*; Kendall/Hunt Publishing Co.: Dubuque, IA, 1996. (b) Volk, T. *CO_2 Rising: The World's Greatest Environmental Challenge*; The MIT Press: Cambridge, MA, 2008. (c) *IPCC Special Report on Carbon Dioxide Capture and Storage*; Metz, B., Davidson, O., de Coninck, H., Loos, M., Meyer, L., Eds.; Cambridge University Press: Cambridge, U.K., 2005.

(2) MacDowell, N.; Florin, N.; Buchard, A.; Hallett, J.; Galindo, A.; Jackson, G.; et al. *Energy Environ. Sci.* **2010**, 1645.

(3) Peuser, I.; Neu, R. C.; Zhao, X.; Ulrich, M.; Schirmer, B.; Tannert, J. A.; Kehr, G.; Fröhlich, R.; Grimme, S.; Erker, G.; Stephan, D. W. *Chem.—Eur. J.* **2011**, *17*, 9640 and references therein.

(4) Mömming, C. M.; Otten, E.; Kehr, G.; Fröhlich, R.; Grimme, S.; Stephan, D. W.; Erker, G. *Angew. Chem., Int. Ed.* **2009**, *48*, 6643 and references therein.

(5) Thompson, R. L.; Hedges, S. W. *Fuel* **2012**, *95*, 655.

(6) Welch, G. C.; Juan, R. R. S.; Masuda, J. D.; Stephan, D. W. *Science* **2006**, *314*, 1124.

(7) Geier, S. J.; Stephan, D. W. *J. Am. Chem. Soc.* **2009**, *131*, 3476.

(8) (a) Otten, E.; Neu, R. C.; Stephan, D. W. *J. Am. Chem. Soc.* **2009**, *131*, 9918. (b) Gilbert, T. M. *Dalton Trans.* **2012**, *41*, 9046.

(9) Kwon, H. J.; Kim, H. W.; Rhee, Y. M. *Chem.—Eur. J.* **2011**, *17*, 6501.

(10) Menard, G.; Stephan, D. W. *Angew. Chem., Int. Ed.* **2011**, *50*, 8396.

(11) Sajid, M.; Klose, A.; Birkmann, B.; Liang, L.; Schirmer, B.; Wiegand, T.; Eckert, H.; Lough, A. J.; Fröhlich, R.; Daniliuc, C. G.; Grimme, S.; Stephan, D. W.; Kehra, G.; Erker, G. *Chem. Sci.* **2013**, *4*, 213.

(12) (a) Duren, M. A.; Stephan, D. W. *J. Am. Chem. Soc.* **2009**, *131*, 8396. (b) McCahill, J. S. J.; Welch, G. C.; Stephan, D. W. *Angew. Chem., Int. Ed.* **2007**, *119*, 5056.

(13) Welch, G. C.; Stephan, D. W. *J. Am. Chem. Soc.* **2007**, *129*, 1880.

(14) (a) Duong, H. A.; Tekavec, T. N.; Arif, A. M.; Louie, J. *Chem. Commun.* **2004**, 112. (b) Iida, K.; Sato, H. *J. Phys. Chem. B* **2012**, *116*, 2244. (c) Theuergarten, E.; Schlösser, J.; Schluns, D.; Freytag, M.; Daniliuc, C. G.; Jones, P. G.; Tamm, M. *Dalton Trans.* **2012**, *41*, 9101. (d) Hounjet, L. J.; Caputo, C. B.; Stephan, D. W. *Angew. Chem., Int. Ed.* **2012**, *51*, 4714. (e) Ashley, A. E.; Thompson, A. L.; O'Hare, D. *Angew. Chem., Int. Ed.* **2009**, *48*, 9839. (f) Stirling, A.; Hamza, A.; Rokob, T. A.; Papai, I. *Chem. Commun.* **2008**, 3148.

(15) (a) Dickie, D. A.; Coker, E. N.; Kemp, R. A. *Inorg. Chem.* **2011**, *50*, 11288. (b) Menard, G.; Stephan, D. W. *Angew. Chem., Int. Ed.* **2011**, *50*, 8396. (c) Chase, P. A.; Jurca, T.; Stephan, D. W. *Chem. Commun.* **2008**, 1701. (d) Chen, D.; Klankermayer, J. *Chem. Commun.* **2008**, 2130. (e) Chen, D. W.; Klankermayer, J. *Angew. Chem., Int. Ed.* **2010**, *49*, 9475.

(16) (a) Stephan, D. W.; Erker, G. *Angew. Chem., Int. Ed.* **2010**, *49*, 46. (b) Stephan, D. W. *Org. Biomol. Chem.* **2008**, *6*, 1535. (c) Stephan, D. W. *Chem. Commun.* **2010**, 8526. (d) Stephan, D. W. *Dalton Trans.* **2009**, 3129.

(17) (a) Rokob, T. A.; Hamza, A.; Stirling, A.; Soos, T.; Papai, I. *Angew. Chem., Int. Ed.* **2008**, *47*, 2435. (b) Hamza, A.; Stirling, A.; Rokob, T. A.; Papai, I. *Int. J. Quantum Chem.* **2009**, *109*, 2416. (c) Rokob, T. A.; Hamza, A.; Papai, I. *J. Am. Chem. Soc.* **2009**, *131*, 10701.

(18) (a) Grimme, S.; Kruse, H.; Goerigk, L.; Erker, G. *Angew. Chem., Int. Ed.* **2010**, *49*, 1402. (b) Schirmer, B.; Grimme, S. *Chem. Commun.* **2010**, *46*, 7942. (c) Mück-Lichtenfeld, C.; Grimme, S. *Dalton Trans.* **2012**, *41*, 9111.

(19) Pu, M.; Privalov, T. *J. Chem. Phys.* **2013**, *138*, 154305.

(20) Bako, I.; Stirling, A.; Balint, S.; Papai, I. *Dalton Trans.* **2012**, *41*, 9023.

(21) Zhao, X.; Stephan, D. W. *J. Am. Chem. Soc.* **2011**, *133*, 12448.

(22) Rocchigiani, L.; Ciancaleoni, G.; Zuccaccia, C.; Macchioni, A. *J. Am. Chem. Soc.* **2014**, *136*, 112.

(23) Devarajan, D.; Doubleday, C. E.; Ess, D. H. *Inorg. Chem.* **2013**, *52*, 8820.

(24) (a) Grimme, S.; Antony, J.; Ehrlich, S.; Krieg, H. *J. Chem. Phys.* **2010**, *132*, 154104. (b) Grimme, S. *J. Comput. Chem.* **2006**, *27*, 1787. (c) Cohen, A. J.; Mori-Sanchez, P.; Yang, W. *Chem. Rev.* **2012**, *112*, 289. (d) Riley, K. E.; Pitonak, M.; Jurecka, P.; Hobza, P. *Chem. Rev.* **2010**, *110*, 5023.

(25) Lourderaj, U.; Park, K.; Hase, W. L. *Int. Rev. Phys. Chem.* **2008**, *27*, 361.

(26) Luk, L. Y. P.; Ruiz-Pernía, J. J.; Dawson, W. M.; Roca, M.; Loveridge, E. J.; Glowacki, D. R.; Harvey, J. N.; Mulholland, A. J.; Tuñón, I.; Moliner, V.; Allemann, R. K. *Proc. Natl. Acad. Sci. U.S.A.* **2013**, DOI: 10.1073/pnas.1312437110 and references therein.

(27) (a) Karplus, M.; McCammon, J. A. *Nat. Struct. Biol.* **2002**, *9*, 646. (b) Glowacki, D. R.; Harvey, J. N. *Nat. Chem.* **2012**, *4*, 169. (c) Loveridge, E. J.; Behiry, E. M.; Guo, J.; Allemann, R. K. *Nat. Chem.* **2012**, *4*, 292. (d) Hay, S.; Scrutton, N. S. *Nat. Chem.* **2012**, *4*, 161.

(28) (a) Siebert, M. R.; Zhang, J.; Addepalli, S. V.; Tantillo, D. J.; Hase, W. L. *J. Am. Chem. Soc.* **2011**, *133*, 8335. (b) Siebert, M. R.; Manikandan, P.; Sun, R.; Tantillo, D. J.; Hase, W. L. *J. Chem. Theory Comput.* **2012**, *8*, 1212.

(29) Hong, Y. J.; Tantillo, D. J. *Nat. Chem.* **2014**, *6*, 104.

(30) Sun, L.; Song, K.; Hase, W. L. *Science* **2002**, *296*, 875.

(31) J. Mikosch, J.; Trippel, S.; Eichhorn, C.; Otto, R.; Lourderaj, U.; Zhang, J. X.; Hase, W. L.; Weidemüller, M.; Wester, R. *Science* **2008**, *319*, 183.

(32) (a) Townsend, D.; Lahankar, S. A.; Lee, S. K.; Chambreau, S. D.; Suits, A. G.; Zhang, X.; Rheinecker, J.; Harding, L. B.; Bowman, J.

M. *Science* **2004**, *306*, 1158. (b) Jordan, M. J. T.; Kable, S. H. *Science* **2012**, *335*, 1054. (c) Grubb, M. P.; Warter, M. L.; Xiao, H.; Maeda, S.; Morokuma, K.; North, S. W. *Science* **2012**, *335*, 1075.
(33) For a review, see: Bowman, J. M.; Shepler, B. C. *Annu. Rev. Phys. Chem.* **2011**, *62*, 531.
(34) (a) Christoffel, K.; Bowman, J. M. *Phys. Chem. A* **2009**, *113*, 4138. (b) McKown, B. G.; Ceriotti, M.; Womack, C. C.; Kamarchik, E.; Butler, L. J.; Bowman, J. M. *J. Phys. Chem. A* **2013**, *117*, 10951.
(35) For a review, see: Skodie, R. T. *Annu. Rev. Phys. Chem.* **1993**, *44*, 145−72.
(36) Pu, M.; Privalov, T. *Int. J. Quantum Chem.* **2014**, *114*, 289.
(37) (a) *The Investigation of Organic Reactions and Their Mechanisms*; Makill, H., Ed.; Wiley-Blackwell: New York, 2007. (b) Hammett, L. P. *Physical Organic Chemistry: Reaction Rates, Equilibria and Mechanisms*, 2nd ed.; McGraw-Hill: New York, 1970. (c) Allen, M. P.; Tildesley, D. J. *Computer Simulations of Liquids*; Claredon Press: Oxford, 1987.
(38) (a) Marx, D.; Hutter, J. *Ab Initio Molecular Dynamics: Basic Theory and Advanced Methods*; Cambridge University Press: Cambridge, U.K., 2009. (b) Billing, G. D.; Mikkelsen, K. V. *Advanced Molecular Dynamics and Chemical Kinetics*; Wiley-Interscience: New York, 1997. (c) Pomerantz, A. E.; Camden, J. P.; Chiou, A. S.; Ausfelder, F.; Chawla, N.; Hase, W. L.; Zare, R. N. *J. Am. Chem. Soc.* **2005**, *127*, 16368. (d) Polanyi, J. C.; Wong, W. H. *J. Chem. Phys.* **1969**, *51*, 1439. (e) Liu, J.; Song, K.; Hase, W. L.; Anderson, S. L. *J. Am. Chem. Soc.* **2004**, *126*, 8602. (f) Carpenter, B. K. *Annu. Rev. Phys. Chem.* **2005**, *56*, 57. (g) Ammal, S. C.; Yamataka, H.; Aida, M.; Dupuis, M. *Science* **2003**, *299*, 1555. (h) Litovitz, A. E.; Keresztes, I.; Carpenter, B. K. *J. Am. Chem. Soc.* **2008**, *130*, 12085. (i) Manikandan, P.; Zhang, J.; Hase, W. L. *J. Phys. Chem. A* **2012**, *116*, 3061. (j) Glowacki, D. R.; Marsden, S. P.; Pilling, M. J. *J. Am. Chem. Soc.* **2009**, *131*, 13896.
(39) Carpenter, B. K. *Annu. Rev. Phys. Chem.* **2005**, *56*, 57.
(40) (a) Xu, L.; Doubleday, C. E.; Houk, K. N. *J. Am. Chem. Soc.* **2010**, *132*, 3029. (b) Xu, L.; Doubleday, C. E.; Houk, K. N. *J. Am. Chem. Soc.* **2011**, *133*, 17848. (c) Black, K.; Liu, P.; Xu, L.; Doubleday, C. E.; Houk, K. N. *Natl. Acad. Sci. U.S.A.* **2012**, *109*, 12860. (d) Xu, L.; Doubleday, C. E.; Houk, K. N. *Angew. Chem., Int. Ed.* **2009**, *48*, 2746.
(41) (a) Ufimtsev, I. S.; Martinez, T. J. *Comput. Sci. Eng.* **2008**, *10*, 26. (b) Ufimtsev, I. S.; Martinez, T. J. *J. Chem. Theory Comput.* **2009**, *5*, 2619. (c) Ufimtsev, I. S.; Martinez, T. J. *J. Chem. Theory Comput.* **2009**, *5*, 1004. (d) Ufimtsev, I. S.; Martinez, T. J. *J. Chem. Theory Comput.* **2008**, *4*, 222.
(42) Henkelman, G.; Uberuaga, B. P.; Jonsson, H. *J. Chem. Phys.* **2000**, *113*, 9901.
(43) Pechukas, P. *Annu. Rev. Phys. Chem.* **1981**, *32*, 159.
(44) (a) Garrett, B. C.; Truhlar, D. G. Variational transition state theory. In *Theory and Applications of Computational Chemistry: The First Forty Years*; Dykstra, C., et al., Eds.; Elsevier B.V.: New York, 2005; pp 67−87. (b) Frenkel, D.; Smit, B. *Understanding Molecular Simulations. From Algorithms to Applications*; Academic Press: Boston, 1996. (c) Bolton, K.; Hase, W. L.; Peslherbe, G. H. Direct dynamics of reactive systems. In *Modern Methods for Multidimensional Dynamics Computation in Chemistry*, Thompson, D. L., Ed.; World Scientific: Singapore, 1998; pp 143−189.
(45) Incidentally, these are modes of motions which are able to couple to the intrinsic reaction coordinate as revealed by the harmonic frequency spectrum calculated at the TS-structure.
(46) The data set comprises 125 AIMD trajectories calculated for 2.5 ps with the time step of 1 fs. The two-dimensional binning uses 0.2 Å/0.2 Å "tiles" on C···P/B···O plane.
(47) (a) Shaik, S.; Maitre, P.; Sini, G.; Hiberty, P. C. *J. Am. Chem. Soc.* **1992**, *114*, 7861. (b) Shaik, S.; Danovich, D.; Wu, W.; Hiberty, P. C. *Nat. Chem.* **2009**, *1*, 443.